Overview of ICRF plasma production and heating in gas mixtures in stellarators

Yurii V. Kovtun [1*], *Vladimir E.* Moiseenko[1,2], *Hiroshi* Kasahara[3], *Tetsuo* Seki[3], *Ryosuke* Seki[3], *Shuji* Kamio[4], *Kenji* Saito[5], *Suguru* Masuzaki[3], *Mikiro* Yoshinuma[3], *Dirk* Hartmann[6], *Jozef* Ongena[7], *Yevgen O.* Kazakov[7], *Tom* Wauters[5], *Andreas* Dinklage[6], *Marcin* Jakubowski[6], *Kristel* Crombé[7], and *Igor E.* Garkusha[1]

[1]Institute of Plasma Physics of the National Science Center "Kharkiv Institute of Physics and Technology", 1, Akademichna St., 61108 Kharkiv, Ukraine
[2]Ångström Laboratory, Uppsala University, 75104 Uppsala, Sweden
[3]National Institute for Fusion Science, 322-6 Oroshi-cho, Toki, Japan
[4]University of California Irvine, Irvine, California 92697, USA
[5]ITER Organization, Route de Vinon-sur-Verdon, CS 90046, 13067 St. Paul Lez Durance Cedex, France
[6]Max-Planck-Institut fur Plasmaphysik, Wendelsteinstraße 1, 17491 Greifswald, Germany
[7]Laboratory for Plasma Physics, ERM/KMS, TEC Partner, 30, Avenue de la Renaissancelaan, 1000 Brussels, Belgium

Abstract. The study of plasma production and heating in the ion cyclotron range of frequencies (ICRF) has a long history in fusion research. The ICRF discharges have been studied in stellarators, tokamaks and mirror devices, mainly. The possibility of efficient additional plasma heating using ICRF is one of the main aims of the studies. Plasma production using ICRF discharges is also studied, but to a lesser extent. For the purpose of wall conditioning in both pure gases and their mixtures has been used with lower RF power level. In support of the ICRF experiments for plasma production at Wendelstein 7-X, studies on the development of an ICRF start-up scenario were initiated on the Uragan-2M (U-2M) stellarator. Experiments with a controlled minority of hydrogen in helium atmosphere showed a significant increase in the resulting plasma density compared with pure helium and pure hydrogen. Then, the ICRF plasma production was demonstrated on the LHD with the scenario based on U-2M experiment. Successful experiments at U-2M and LHD showed that the ICRF start-up scenario can be scaled up to large stellarator devices, producing plasma with favorable parameters from scratch using ICRF only.

1 Introduction

One of the most important goals in controlled thermonuclear fusion is to produce dense plasma and heat it to high temperatures at which thermonuclear reactions can occur [1, 2]. Currently, in toroidal thermonuclear devices with magnetic plasma confinement, three methods of plasma production and heating are most widely used: Neutral Beam Injection (NBI) heating, Electron Cyclotron Resonance Heating (ECRH), and Ion Cyclotron Resonance Heating (ICRH) [3]. In modern tokamaks and stellarators, several methods of plasma production and heating are usually used [4-6]. This provides flexibility when conducting experiments with high-temperature plasma. The superconducting tokamak currently under construction as the International Thermonuclear Experimental Reactor (ITER) project also plans to use ECRH, ICRH, and NBI [7].

ICRH research in toroidal thermonuclear devices has a long history [8-10]. The first ICRH experiments were conducted on the Model C stellarator [11]. Later, many ICRH experiments were conducted on both stellarators [12] and tokamaks [13]. Currently, there are three main functions for ICRH. The first is the use of ICRH for additional heating of plasma produced and heated by other methods, such as ECRH or NBI. Various heating schemes and scenarios are used for plasma heating, for example three-ion [14]. ICRH has also been used in experiments with thermonuclear fuel in deuterium–tritium experimental campaigns at the Joint European Torus (JET) tokamak [15, 16]. The second task is to sustain the plasma that was previously produced by ECRH or NBI. Such experiments have been carried out numerous times on the Wendelstein 7-AS (W7-AS) [17], Compact Helical System (CHS) [18], and LHD [19] stellarators. Moreover, scenarios with long-pulse discharge lasting ICRH (0.4 MW) and ECRH (0.1 MW) up to 54 min were implemented on LHD [20]. The third

* Corresponding author: Ykovtun@kipt.kharkov.ua

task is to produce and heat plasma using only ion cyclotron range of frequencies (ICRF) discharges. This is done both to obtain hot and dense plasma and to obtain plasma for wall conditioning procedures [21].

This paper summarizes both previous results and presents new studies on ICRF plasma production in gas mixtures. The main focus is on experimental results obtained on U-2M and LHD.

2 ICRF discharge

The study of plasma production by ICRF discharges has previously been conducted in toroidal magnetic traps, tokamaks, stellarators, and mirror traps. In tokamaks, ICRF discharges are used during wall conditioning procedures [21, 22]. In this case, they are ignited in a toroidal magnetic field and, accordingly, there are no closed magnetic surfaces. In stellarators, ICRF discharges find application in plasma production and heating [23-29], as well as for wall conditioning [30]. In pure gases, experiments on the production of radio frequency (RF) discharge plasma were conducted in the CHS [23], W7-AS [24], LHD [25], Uragan-3M (U-3M) and Uragan-2M (U-2M) [26, 27], and H-1 [28, 29] stellarators. They demonstrated the possibility of producing plasma with a density of 10^{18}–10^{19} m^{-3} and a temperature ranging from several tens to hundreds of eV.

One of the features of realising RF discharges in magnetic traps is the presence of a gas breakdown stage and plasma creation. The RF breakdown stage was experimentally investigated in [31–33]. Experiments show that the breakdown time depends on pressure, magnetic field, RF breakdown voltage, etc. Numerical simulation of RF breakdown using 1D particle-in-cell Monte Carlo collision (PIC-MCC) code was performed in [34]. Simulation of RF plasma production was performed in [26, 35, 36]. Theoretical consideration of RF plasma production was also discussed in [37, 38].

Most experimental and theoretical studies and simulations were conducted for pure gases. However, studies were conducted on the creation of plasma in gas mixtures, including mixtures of helium and hydrogen. Thus, the 0D model of magnetized hydrogen–helium wall conditioning plasmas was used in [39]. In the TEXTOR and ASDEX Upgrade tokamaks, ICRF discharges in He+H_2 mixtures were used for wall conditioning [40-43]. In these experiments, a plasma density of 10^{16}–5×10^{17} m^{-3} was observed. In experiments on He/H fuelling changeover at JET, plasma with a density of up to ~2×10^{17} m^{-3} was observed in helium ICRF discharge with hydrogen minority higher than in hydrogen ICRF discharge [44]. The emission H_α was also observed in the cyclotron resonance region for hydrogen in the helium ICRF discharge.

Experiments on the production of ICRF plasma in a mixture of hydrogen and helium were also conducted on the Phaedrus-B tandem mirror [45] and HIEI axisymmetric single mirror [46]. In experiments [45], a significant increase in plasma energy density was observed in the case of a mixture compared to those obtained under the same conditions with pure hydrogen plasma.

In stellarators, research on ICRF discharges in He+H_2 mixtures was conducted in Sirius [47] and H-1NF (H-1) [28, 29, 48]. Higher plasma density was achieved in He+H_2 mixtures compared to pure hydrogen in H-1 [48]. The plasma density was ~2×10^{18} m^{-3} and electron temperatures of several tens of eV have been observed with injected RF power up to 80 kW in experiments on H-1NF [48]. For completeness, note that the He+H_2 mixture was also used in ICRF sustain the plasma experiments on LHD [19].

The studies of ICRF discharges in He+H_2 mixtures show that higher plasma parameters are achieved in mixtures than in ICRF discharges in hydrogen. However, high values of density and temperature were not achieved when producing ICRF discharges plasma.

3 ICRF plasma production in gas mixtures in Uragan-2M stellarator

3.1 Uragan-2M stellarator

The Uragan-2M (U-2M) device at Kharkiv, Ukraine, is a medium-size stellarator of the torsatron type [49, 50]. The U-2M magnetic system consists of the $l = 2$ helical coils with four periods ($m = 4$) in the toroidal direction, 16 toroidal field coils evenly distributed along the torus and 8 poloidal coils (see Fig. 1). The magnetic configuration can be changed by varying the parameter $K_\phi = B_{th} /(B_{tt} + B_{th})$ where B_{tt} and B_{th} are the toroidal fields at the geometrical axis of the torus produced by the toroidal and helical coils, respectively. Plasma diagnostics include: time-resolved optical emission spectroscopy, microwave interferometer, Langmuir probes and other diagnostic methods. The location of the plasma diagnostics is shown in Fig. 1a. Plasma is created and heated by a two strap antenna installed is mimicking the W7-X ICRH antenna (see Fig. 1c). The antenna was connected to the Kaskad-1 RF system [50]. A gas mixture system on U-2M was used to prepare a gas mixture of a specified composition [51]. This allowed experiments to be conducted with a controlled percentage of gases of the mixture. The mixture was analyzed by a mass spectrometer before and after the experiments ICRF plasma production. The main technical details of U-2M device are summarized in Table 1, in detail presented in [49, 50].

3.2 Experimental results at Uragan-2M

Experiments on ICRF plasma production were conducted at several experimental campaigns on U-2M during 2019-2021. In the experiments here, the two strap antenna operated in monopole phasing [0 0]. To control RF power, the RF generator anode voltage U_a is varied stepwise as follows: $U_{a1} = 0.4U_a$ at the start, $U_{a2} = 0.6\,U_a$ at step 1, and the maximum anode voltage U_a was set at step 2. The RF frequency was equal to the fundamental hydrogen cyclotron harmonic $\omega_{RF} \approx \omega_{ci}(H^+) \approx 2\omega_{ci}(He^{2+}) \approx 2\omega_{ci}(D^+) \approx 4\omega_{ci}(He^+)$.

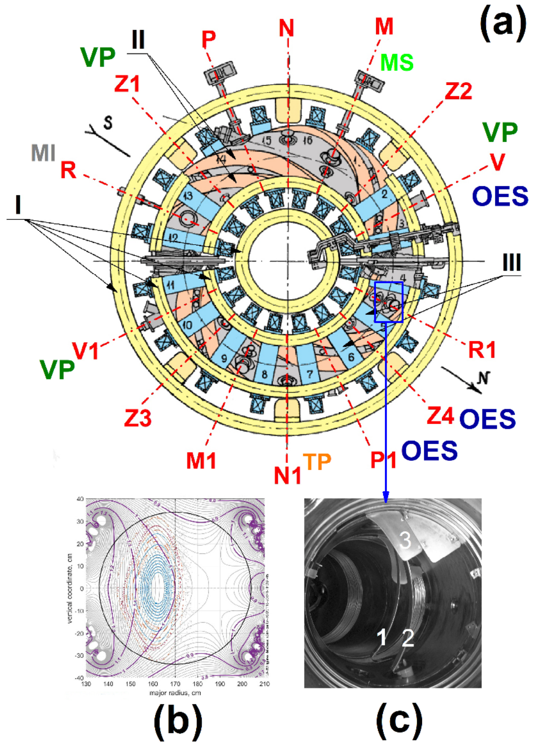

Fig. 1. (a) General view of stellarator Uragan-2M. I the poloidal field coils; II the helical field coils; III the toroidal field coils (numbered 1–16). Different toroidal cross-sections are shown by red lines and denoted by capital letters and numbers. The blue square is the location of the antenna. OES - optical emission spectroscopy, VP - vacuum pumps, MS - mass spectrometer, MI - microwave interferometer, TP - triple probe. (b) Poincaré plot of magnetic configuration and contours of magnetic field module at U-2M in antenna location. The circular line shows the vacuum chamber wall. (c) General view of two-strap antenna in U-2M vacuum chamber. 1 and 2 straps, 3 antenna limiter.

Table 1. U-2M Devices characteristics.

Parameter	**Value**
Major radius, R (m)	1.7
Minor radius, r (m)	0.34
Plasma volume, V_p (m^3)	~ 1.6
Magnetic field, B (T)	< 0.6 (max 2.5)
Plasma heating tools	ICRF
Total heating power, (MW)	< 0.4

3.2.1 ICRF production of plasma in He+H_2

The first experiments on ICRF plasma production were conducted using pure helium [49]. A small amount of hydrogen was constantly present in the vacuum chamber during these experiments. The experiments demonstrated the possibility of reliably producing ICRF discharge plasma using a two-strap antenna in the pressure range p = (4–14)×10^{-2} Pa. The plasma density reached up to 2×10^{18} m^{-3}. Increasing the input power did not lead to a significant increase in density at constant pressure. Although the hydrogen was not supplied, the magnetic field scan demonstrated crucial role on its presence in plasma.

The first experiments with controlled minority hydrogen concentration were conducted in [52]. The hydrogen minority control allowed one to increase plasma density more than three times as compared with pure helium. The developed scenario allowed to decrease the neutral gas pressure at which the plasma production is possible. A plasma density of 9×10^{18} m^{-3} was achieved at a pressure of 8.3×10^{-3} Pa in 86%He+ 14%H_2 [52]. In these experiments, the mixture was produced inside a vacuum chamber with a constant flow of helium and hydrogen. This method did not allow the percentage of gases to be maintained accurately enough, especially when it was necessary to change the pressure in the vacuum chamber. Therefore, to fix this, a gas mixture system was developed and used in all subsequent experiments [51]. This made it possible to conduct experiments with different gas mixtures and gas concentrations at any required pressure.

Further experiments were conducted in the range of initial hydrogen concentrations from 4% to 75% in the mixture and in the pressure range from 6×10^{-4} Pa to 1.5×10^{-1} Pa [50, 53-55]. A representative ICRF shot is shown in Fig. 2. At the first stage of the ICRF discharge, an RF breakdown occurred, which was characterized by the appearance of the intensity of the hydrogen spectral line and a delay in the helium line. This was followed by an increase in plasma density. The second stage was quasi-stationary, with slight changes in plasma parameters. And the third stage, after the RF power is turned off, is the decay and collapse of the plasma. Experiments have shown that under the same initial conditions, the plasma density in He+H_2 is higher than in pure hydrogen and pure helium (see Fig. 3) [50, 54, 55].

In the region $\omega_{RF} \approx \omega_{ci}$ (H^+), the maximum plasma density is observed when the ion cyclotron condition for hydrogen is met in plasma. An increase or decrease in the magnetic field value leads to a significant decrease in plasma density by an order of magnitude [55]. The maximum plasma density in He+H_2 achieved in experiments depended on the hydrogen concentration. The maximum dense plasma was observed at a hydrogen concentration of 14% in the mixture. With an increase in the hydrogen concentration in the mixture, the observed plasma density values decreased under the same initial conditions (see fig. 4). The maximum plasma density observed was up to 1×10^{19} m^{-3}, and with an additional pulse injection of hydrogen, up to 1.3×10^{19} m^{-3} [56]. The RF power density at the level of 60 kW/m^3 is necessary to produce a plasma with relatively high density [54, 55]. However, in all experiments, a low electron temperature of ~10–40 eV was observed [53, 55]. The ion temperature was also low, ≈18–23 eV [53, 55]. The presence of impurity ions of carbon and oxygen

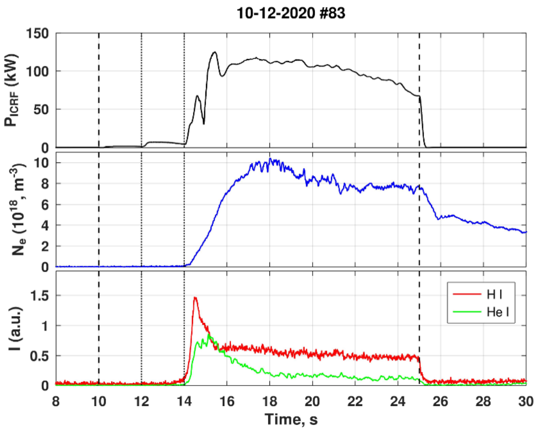

Fig. 2. Time evolutions of RF power; average plasma density; optical emission intensities of H_α (656.2 nm), He I, (447.15 nm). ($U_a = 8$ kV, f = 4.9 MHz, $B_0 = 0.35$ T, $K_\phi = 0.32$, working gas 14%H_2 + 86%He, p = 8.4 × 10^{-3} Pa. The vertical lines show characteristic time moments of duty cycle of RF generator). The experimental data [53].

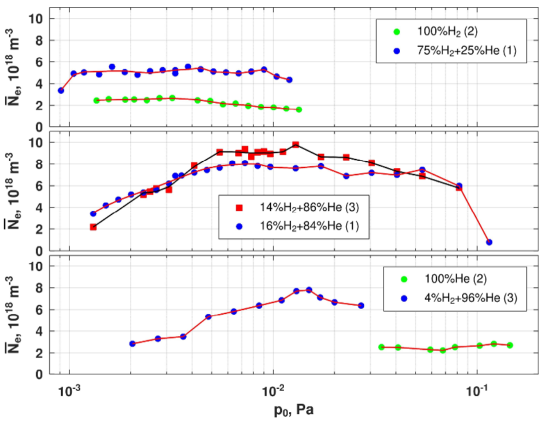

Fig. 3. Average plasma density as a function of the pressure. Data of this experimental series (1) [55], and (2) [50, 54] and (3) [53] (f = 4.9 MHz and $U_a = 7$ kV, RF power ≈100 kW).

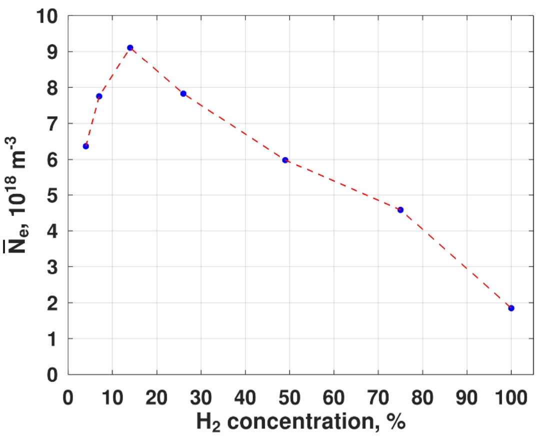

Fig. 4. Average plasma density as a function of the of the initial hydrogen concentration in the mixture. (f = 4.9 MHz, U_a = 7 kV, p ~ 8×10^{-3} Pa).

with Z = 1 and 2 was observed in the plasma. Ions with high charge were not observed due to the low electron temperature.

Experiments conducted in [55, 57] demonstrated the possibility of producing plasma in a He+H_2 mixture using ICRF discharge at the second harmonic of cyclotron resonance for hydrogen $\omega_{RF} \approx 2\omega_{ci}$ (H^+). However, the plasma density was several times lower than that created by ICRF discharge at $\omega_{RF} \approx \omega_{ci}$ (H^+) and was below the value of 3×10^{18} m^{-3}.

In [56], a supersonic hydrogen molecular beam was injected into helium plasma using ICRF discharge injection. As a result of hydrogen ionization in the plasma volume, a mixture of He+H was produced. The maximum average density of helium plasma was increased 2.1 times up to 4×10^{18} m^{-3} after supersonic molecular beam injection pulse.

Some aspects of electromagnetic wave propagation in plasma for the conditions of experiments conducted on U-2M were considered in [49, 55]. The lower density threshold is determined for slow waves SW under the condition $k_{\perp,SW} = 0$ ($k_\perp$ is the perpendicular wavenumber), above which SW propagation is possible. As can be seen from Fig. 5, the threshold density value is practically the same for pure helium, hydrogen, and their mixture. In the case of helium, the upper limit of plasma density above which SW cannot propagate is determined by the lower hybrid resonance condition, $k^2_{\perp,SW} \to \infty$. In the case of hydrogen and the He+H mixture, this is not true. With increasing density, fast waves (FW) can propagate above the critical density, the value of which is determined by $k_{\perp,FW} = 0$. A further increase in density in the case of hydrogen and the He+H mixture leads to the possibility of FW conversion to SW at the conversion point (Alfvén resonance) [49, 58]. Moreover, in the He+H mixture, the conversion point is located in a region of higher density than in hydrogen (see Fig. 5).

As a result, the main requirement for the ICRF plasma production scenario is the presence of hydrogen ions and an ion cyclotron resonance zone for ω_{ci} (H^+)inside the plasma column [49, 55]. The main mechanism of plasma formation is the ionization of neutral atoms (molecules) under the influence of electrons. At low plasma densities, electrons are heated by SW absorption by the plasma. At higher plasma densities, FW propagates. In the layer where the Alfvén resonance condition is satisfied, FW is converted into SW. The SW propagates in the direction of the lower hybrid resonance (LHR) layer, where SW is completely absorbed [49].

In conclusion, we note that in experiments on ICRF plasma production in an He+H_2 mixture on U-2M, a plasma density of 10^{19} m^{-3} was achieved, which is significantly higher than what was previously obtained in tokamaks and stellarators (see Section 2).

3.2.2 ICRF production of plasma in He+H_2+D_2

In [50], ICRF plasma production in a three-component mixture of He+H_2+D_2 was investigated. In He+H_2+D_2, a similar pattern was observed as in the two-component mixture of He+H_2, namely, the maximum density was observed when the RF frequency was close to the fundamental hydrogen cyclotron harmonic. Studies show that the ICRF plasma production scenario developed for the He+H_2 mixture [52-56] can be used in the three-component mixture He+H_2+D_2. However, experiments were conducted only in a mixture of

80%He+10%H_2+10%D_2, and it is still necessary to investigate the plasma parameters from different gas concentrations in the three-component mixture, as was done for the He+H_2 mixture in [53-55].

3.2.3 ICRF production of plasma in D_2+H_2

The ICRF plasma production scenario in the He+H_2 mixture was used for the D_2+H_2 mixture in [50]. However, in the 86%D_2+14%H_2 mixture, a density of only 5×10^{16} m^{-3} was achieved. Increasing the hydrogen concentration by more than ~ 50% in the mixture significantly increased the density of the plasma produced. In this case, the plasma density achieved was the same as in pure hydrogen, ≈ 10^{18} m^{-3}. These results are surprisingly poor and, additional research is required.

3.2.4 ICRF production of plasma in Ar+H_2

In experiments [50, 52-57] on ICRF plasma production, the main ions were helium and deuterium. To check how sensitive the minority ICRF plasma production scenario is to the background ion sort, a series of experiments was carried out on U-2M. As plasma majority ions, argon ions were chosen which are much heavier than deuterium and helium. The first experiments on ICRF plasma production were conducted in a mixture of 91%Ar+9%H_2 [59]. Plasma production with an average plasma density up to ~ 4×10^{18} m^{-3} was observed. The plasma parameters were measured for different values of gas pressure and RF power. An increase in the injected RF power, which, in this case, is proportional to the anode voltage in the RF generator, leads to an increase in the plasma density. The plasma density obtained in the argon-hydrogen mixture is higher than in pure hydrogen which is characteristic.

4 ICRF plasma production and heating in Large Helical Device

4.1 Large Helical Device

The Large Helical Device (LHD) is a large-scale heliotron-type superconducting device (see fig. 6a) at Toki, Japan [60]. The poloidal and toroidal period field period numbers are *l/m* = 2/10. The LHD uses three systems to produce and heat plasma: ECRH, NBI and ICRF. The ICRF heating is used with a fixed frequency of 38.47 MHz [61]. The maximum output power is 3 MW. There are two types of antennas on the LHD: a Hand-Shake form antennas (HAS) (see fig. 6b) [62] and a Field-Aligned-Impedance Transforming (FAIT) antennas (see fig. 6c) [63]. The HAS and FAIT antennas are located at ports 3.5 and 4.5, respectively. The antennas occupy the upper (U) and lower (L) ports of the LHD vacuum chamber. All the straps are shielded by the Faraday screens. The RF power can be injected independently in each of the two straps (U) and (L) of these antennas. In the case of using only one strap of one of the antennas, for example HAS (L) and FAIT (L), the antennas are essentially single-strap antennas. When us

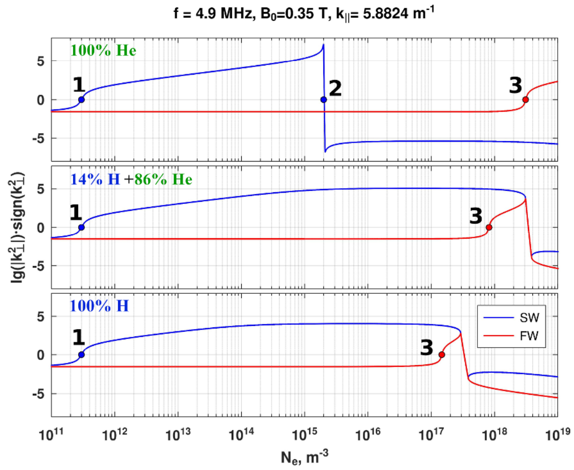

Fig. 5. The squared perpendicular wave numbers of slow waves (SW) and fast waves (FW) of 4.9 MHz frequency as a function of the plasma density, in He, He+H mixture, and H. The numbers correspond to 1 - cutoff SW, 2 - lower hybrid resonance, and 3 - cutoff FW.

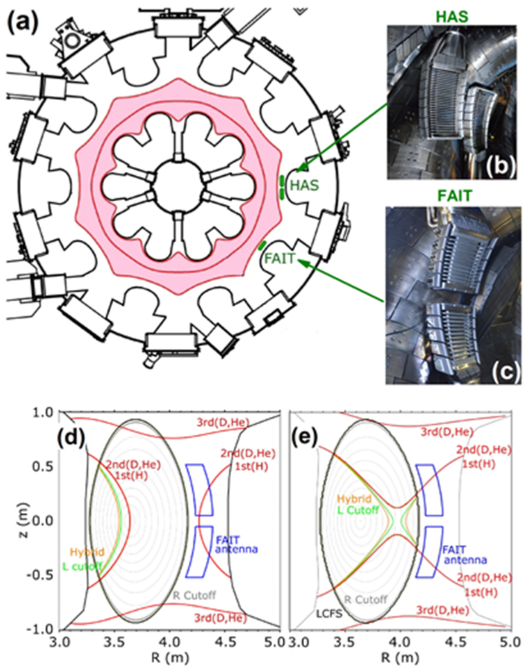

Fig. 6. (a) Schematic view of the mid-plane cross-section of LHD. (b) General view of HAS antenna in LHD vacuum chamber. (c) General view of FAIT antenna in LHD vacuum chamber. LHD cross-section at FAIT antenna location. Last closed flux surface, magnetic surfaces, ion cyclotron resonance layers for R_{ax} = 3.6 m, (d) B_t = 2.55 T, and (e) B_t = 2.75 T.

using two straps (U) and (L) HAS antenna, dipole phasing [0 π] is realized.

Two modes of gas fueling to the LHD vacuum chamber were used: continuous mode of gas fueling (CGF) and pulsed mode of gas fueling (PGF). In CGF mode, hydrogen and helium were injected independently until the required pressure was reached. Accordingly, He+H_2 mixtures were created inside the vacuum vessel. The percentage content of hydrogen and helium was monitored by a mass spectrometer. In PGF mode, in addition to the continuous injection of hydrogen and helium, pre-programmed helium injection was also used.

Table 2. LHD Devices characteristics.

Parameter	Value
Major radius, R (m)	3.9
Minor radius, r (m)	0.6
Plasma volume, V_P (m^3)	~ 30
Magnetic field, B (T)	3
Plasma heating tools	ECRH, NBI, ICRF
Total heating power, (MW)	36

In the experiments, the magnetic field is 2.55 T or 2.75 T at the magnetic axis. In both cases, the cyclotron zone was located inside the plasma column (see fig. 6 d and e). The main technical details of LHD device are summarized in Table 2.

4.2 Experimental results at Large Helical Device

Experiments on ICRF plasma production were conducted within the 22th - 25th experimental campaigns on LHD. The ICRF plasma production scenario developed on the U-2M (see Section 3) was implemented on the LHD. The main differences between the experiments at LHD and at U-2M were the significantly higher magnetic field and larger plasma volume in LHD and higher RF power.

4.2.1 ICRF production of plasma in He+H_2

First experiments (22nd experimental campaign on LHD) on ICRF plasma production in He+H_2 mixture and a magnetic field of 2.55 T. CGF mode was used for gas injection. The RF power was low, below 300 kW [64]. This limitation was introduced to reduce the possibility of arcing in the RF system components. Two scenarios were investigated. In the first (ECRH+ICRF), pre-plasma was created by ECRH discharge is used before the RF pulse. This scenario ensures stable breakdown for ICRF discharges. Since very low-density plasma has already been created, this makes it easier to achieve breakdown and plasma creation. In the second scenario (ICRF), plasma was created only by ICRF discharges. In both scenarios, stable breakdown and plasma production were observed. However, the plasma density was low. When using ICRF discharges and RF power up to 200 kW, plasma with a density of up to 9.5×10^{17} m^{-3} was observed. The electron temperature was apparently low. No dangerous voltage increase at the RF system elements and no arcing has been detected. This made it possible to increase the RF power in subsequent experiments on ICRF plasma production.

In subsequent experiments (23rd experimental campaign on LHD), the injected RF power was significantly increased [54, 65]. The increase was made slowly, keeping low voltage at gas breakdown stage. The experiments were conducted in magnetic fields of 2.55 T and 2.75 T. Thus, in the ECRH+ICRF scenario at a power of 1.75 MW, a density of up to 10^{19} m^{-3} was observed [65]. When plasma was created using only ICRF, a density of 6×10^{18} m^{-3} was achieved, which is 6 times more than in previous experiments. In the ICRF+NBI scenario, where additional perpendicular NBI power was injected into the plasma produced by ICRF, there was no increase in plasma density and temperature. Common to these experiments was the production of low-temperature ICRF plasma. The presence of impurities, such as carbon and oxygen, in plasma leads to radiation losses of more than 0.25 MW. Unlike the experiments on U-2M, excited ions O^{4+*} (O V) and O^{5+*} (O VI) were recorded in the plasma on LHD. Apparently, the electron temperature of the plasma in LHD was slightly higher than that in U-2M. However, the plasma remained cold, T_e < 100 eV. A comparison of the maximum average density obtained on the U-2M and LHD for these modes is shown in Fig. 7. The dependence of density on RF power density is practically linear. To obtain cold dense plasma up to 10^{19} m^{-3}, approximately 60 kW/m^3 is required. However, such plasma can be used for subsequent heating using NBI, as well as for wall conditioning procedures.

In experiments [65], the ECRH + NBI + ICRF scenario was also implemented. In this scenario, plasma was created by ECRH and subsequently supported at the beginning by NBI and then only by ICRF. At the same time, when ICRF was injected, heating of the electron and ion components to ~2 keV was observed. This demonstrated that the task of plasma density ramp-up from the achieved value to representative for LHD may open a way for usage of ICRF for plasma production and heating.

4.2.2 ICRF production and heating of plasma in He+H_2

ICRF plasma production experiments in the 24th experimental campaign on LHD were conducted in a magnetic field of 2.75 T. Both CGF mode and PGF mode were used for gas injection. In these experiments, the possibility of ICRF production and heating of plasma in He+H_2 was demonstrated for the first time [66, 67]. As an example, Fig. 8 shows the plasma parameters for one of the shots. It can be seen that at a low RF power of ≈ 320 kW during the plasma creation stage, heating is also possible, which is characterized by an increase in plasma energy content. Further helium injection (PGF mode) allowed for an increase in plasma density and plasma energy content. Heating was observed both when using gas injection in PGF mode and CGF mode. Unlike previous experiments on ICRF plasma production, a plasma density of ≈ 1×10^{19} m^{-3} and an electron temperature of 2–2.5 keV were observed. The intensity of the spectral lines of carbon, oxygen, and

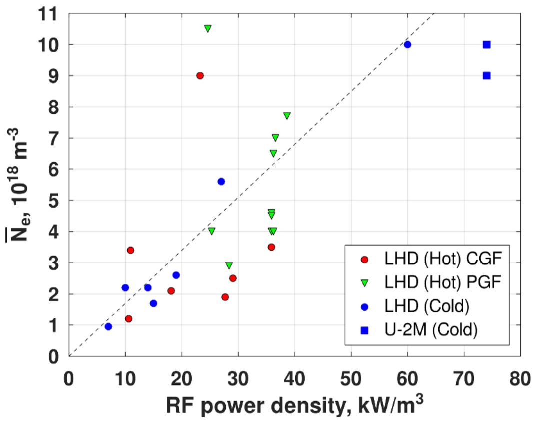

Fig. 7. Dependence of maximum plasma density on RF power density in LHD and U-2M. LHD (Cold) and U-2M (Cold) T_e < 100 eV the experimental data [54]. LHD (Hot) T_e >> 100 eV. CGF continuous mode of gas fueling, PGF pulsed mode of gas fueling.

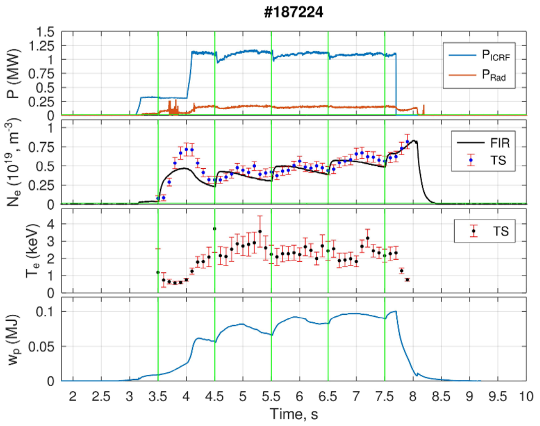

Fig. 8. Time evolutions of the injected power P_{ICRF} (total), radiation power P_{rad}, electron density N_e, and electron temperature T_e and plasma energy content w_p. The vertical green lines indicate gas puff moments. The data average electron density of far-infrared (FIR) laser interferometer at R = 3.669 m, electron density, and temperature of Thomson scattering (TS) at R = 3.602 m are given. The initial working gas content is ~16% H_2 + 84% He.

iron impurities was low, and radiation losses were less than 0.25 MW.

A comparison of the maximum density of cold (T_e < 100 eV) plasma obtained in previous experiments and hot plasma (T_e >> 100 eV) is shown in Fig. 7. It can be seen that in the RF power density range of 10-40 kW/m^3, hot plasma with a density comparable to that obtained for cold plasma can be obtained. For some shots, the RF power density was 23-25 kW/m^3 to produce plasma with a maximum density of (0.9-1.05)$\times 10^{19}$ m^{-3} and heat it. At the same time, for thecase of cold plasma production, this value was 60 kW/m^3.

Dependence of maximum plasma energy content on RF power density showed in fig. 9. It is apparent that higher plasma energy content values can be achieved with increased RF power density. A more promising approach is to use PGF mode for gas injection, which achieves higher plasma energy content values of up to ≈ 100 kJ.

Analysis of wave propagation in cold plasma for LHD experimental conditions shows that in the case of plasma containing He^{2+}+H^+ ions, the plasma density at

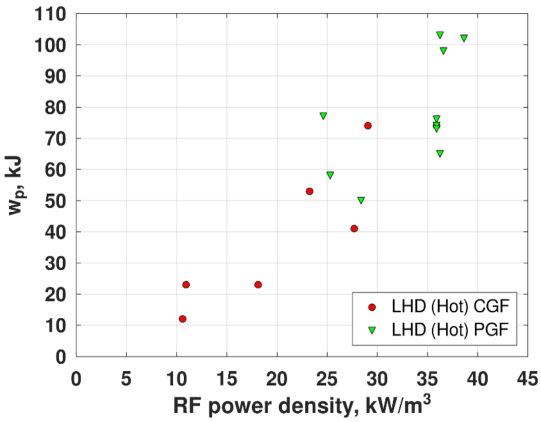

Fig. 9. Dependence of maximum plasma energy content on RF power density in LHD. LHD (Hot) T_e >> 100 eV. CGF continuous mode of gas fueling, PGF pulsed mode of gas fueling.

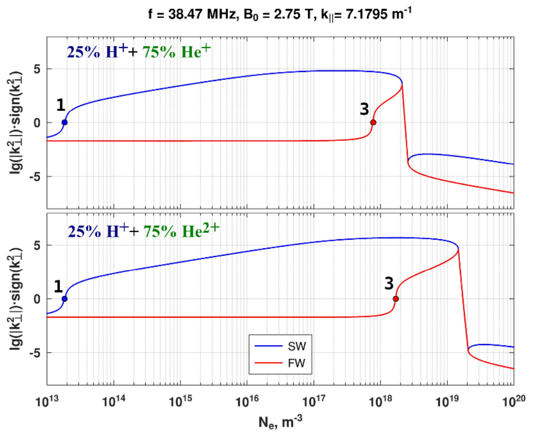

Fig. 10. The squared perpendicular wave numbers of slow waves (SW) and fast waves (FW) of 38.47 MHz frequency as a function of the plasma density, in He+H mixture. The numbers correspond to 1 - cutoff SW and 3 - cutoff FW.

which mode conversion is possible is significantly higher than in the case of plasma containing He^++H^+ (see Fig. 10). Naturally, in the experiment, the wave propagation pattern is dynamic and more complicated.

In subsequent experiments in the 25th experimental campaign on LHD, the main focus was on improving the parameters of plasma production ICRF discharge. The following was achieved: plasma energy content ≈ 158 kJ, plasma density in some shots was higher than 1 × 10^{19} m^{-3}, maximum electron temperature at the center was up to 2.5 keV, maximum ion temperature was observed up to 2-3 keV.

5 Conclusions

The ICRF plasma start-up scenario developed at the U-2M can be scaled up on large stellarators. Stable breakdown and ICRF plasma production is observed. Two modes of plasma production can be realized: first producing a cold plasma that can be used or a wall conditioning procedure, and second producing and heating the plasma. Thus, the implementation of the ICRF production and heating of plasma in He+H_2 scenario on the LHD made it possible to achieve a plasma density of up to 1 × 10^{19} m^{-3} and electron and ion temperatures of several keV. This scenario can be used to create hot plasma in stellarators when other methods of production and heating are not available.

The data supporting the findings of this study are available in the LHD experiment data repository at https://doi.org/10.57451/lhd.

This work has been carried out within the framework of the EUROfusion Consortium, funded by the European Union via the Euratom Research and Training Programme (Grant Agreement No. 101052200—EUROfusion). Views and opinions expressed are however those of the author(s) only and do not necessarily reflect those of the European Union or the European Commission. Neither the European Union nor the European Commission can be held responsible for them.

The work is supported by the National Research Foundation of Ukraine under Grant No. 261/0101 “Critical issues for stellarators as fusion machines”, as a result of the “Excellent Science in Ukraine” competition.

The work is supported by the Ministry of Education and Science of Ukraine (grant PH/56 – 2024).

We are pleased to acknowledge the assistance of the LHD Experiment Group.

The views and opinions expressed herein do not necessarily reflect those of the ITER Organization.

References

1. A. Fasoli, Essay: Overcoming the obstacles to a magnetic fusion power plant, Phys. Rev. Lett. **130**, 220001 (2023). https://doi.org/10.1103/PhysRevLett.130.220001
2. K. H. Nordlund, European Research Roadmap to the Realisation of Fusion Energy (Programme Manager, EUROfusion, Garching/Munich, Germany, 2018)
3. T. Okazaki, Fusion Reactor Design: Plasma Physics, Fuel Cycle System, Operation and Maintenance (Wiley-VCH GmbH, Weinheim, 2022)
4. F. G. Rimini et al., 40 years of JET operations: a unique contribution to fusion science, Plasma Phys. Control. Fusion **67**, 033001 (2025). https://doi.org/10.1088/1361-6587/adaee5
5. M. Endler et al., Wendelstein 7-X on the path to long-pulse high-performance operation, Fusion Eng. Des. **167**, 112381 (2021). https://doi.org/10.1016/j.fusengdes.2021.112381
6. M. Osakabe et al., Current Status of Large Helical Device and Its Prospect for Deuterium Experiment. Fusion Sci. Technol. **72**, 199 (2017). https://doi.org/10.1080/15361055.2017.1335145
7. P. Barabaschi et al., ITER progresses into new baseline, Fusion Engineering and Design **215**, 114990 (2025). https://doi.org/10.1016/j.fusengdes.2025.114990
8. J. C. Hosea, Foundations of ICRF heating - A historical perspective, AIP Conf. Proc. **314**, 128 (1994). https://doi.org/10.1063/1.46748
9. J.-M. Noterdaeme, Fifty years of progress in ICRF, from first experiments on the model C stellarator to the design of an ICRF system for DEMO, AIP Conf. Proc. **2254**, 020001 (2020). https://doi.org/10.1063/5.0014254
10. J. Hillairet, Review on recent progress in ion cyclotron range of frequency systems, experiments and modelling for magnetic confinement fusion, Rev. Mod. Plasma Phys. **7**, 16 (2023). https://doi.org/10.1007/s41614-023-00116-5
11. M. A. Rothman et al., Ion Cyclotron Heating in the Model C Stellarator Available to Purchase, Phys. Fluids **12**, 2211 (1969). https://doi.org/10.1063/1.1692332
12. T. Watari, RF heating in stellarators, Plasma Phys. Control. Fusion **40**, A13 (1998). https://doi.org/10.1088/0741-3335/40/8A/003
13. A. Becoulet, Heating and current drive regimes in the ion cyclotron range of frequency. Plasma Phys. Control. Fusion **38**, A1 (1996). https://doi.org/10.1088/0741-3335/38/12A/002
14. Ye. O. Kazakov et el., Physics and applications of three-ion ICRF scenarios for fusion research, Phys. Plasmas **28**, 020501 (2021). https://doi.org/10.1063/5.0021818
15. P. Jacquet et al., ICRH operations during the JET tritium and DTE2 campaigns, Nucl. Fusion **64**, 066039 (2024). https://doi.org/10.1088/1741-4326/ad3f2c
16. A. Kappatou et al., Overview of the third JET deuterium-tritium campaign, Plasma Phys. Control. Fusion **67**, 045039 (2025). https://doi.org/10.1088/1361-6587/adbd75
17. D. A. Hartmann et al., ICRF results from W7-AS, AIP Conference Proceedings **403**, 49 (1997). https://doi.org/10.1063/1.53339
18. T. Watari et al., RF heating experiments in CHS and RF development for LHD, AIP Conference Proceedings **403**, 57 (1997). https://doi.org/10.1063/1.53392
19. T. Watari et al., The performance of ICRF heated plasmas in LHD, Nucl. Fusion **41**, 325 (2001). https://doi.org/10.1088/0029-5515/41/3/310
20. H. Kasahara et al., Development of steady-state operation using ion cyclotron heating in the Large Helical Device, Phys. Plasmas **21**, 061505 (2014). https://doi.org/10.1063/1.4884363
21. T. Wauters et al., Wall Conditioning in Fusion Devices with Superconducting Coils, Plasma Phys. Controlled Fusion **62**, 034002 (2020). http://doi.org/10.1088/1361-6587/ab5ad0.
22. D. Douai et al., Recent results on ion cyclotron wall conditioning in mid and large size tokamaks, J. Nucl. Mater. **415**, S1021 (2011). https://doi.org/10.1016/j.jnucmat.2010.11.083

23. K. Nishimura et al., Compact helical system physics and engineering design, Fusion Technol. **17**, 86 (1990). https://doi.org/10.13182/FST90-A29173
24. W. Ballico et al., Minority Heating Experiments on the W7-AS Stellarator, AIP Conference Proceedings **244**, 150 (1992). https://doi.org/10.1063/1.41687
25. Y. Torii et al., Plasma production experiments using a folded waveguide antenna on LHD, Nucl. Fusion **42**, 679 (2002). https://doi.org/10.1088/0029-5515/42/6/306
26. V. E. Moiseenko et al., RF plasma production and heating below ion cyclotron frequencies in Uragan torsatrons, Nucl. Fusion **51**, 083036 (2011). https://doi.org/10.1088/0029-5515/51/8/083036
27. V. E. Moiseenko et al., Characteristics of regular discharges in Uragan-3M torsatron, Plasma Phys. Controlled Fusion **61**, 065006 (2019). https://doi.org/10.1088/1361-6587/ab140d
28. B. D. Blackwell, Results from helical axis stellarators, Phys. Plasmas **8**, 2238 (2001). https://doi.org/10.1063/1.1364671
29. B. D. Blackwell et al., Overview and results from the H-1 National Facility, AIP Conf. Proc. **669**, 158 (2003). https://doi.org/10.1063/1.1593890
30. R. Brakel et al., ICRF wall conditioning experiments in the W7-AS stellarator, J. Nucl. Mater. **290–293**, 1160 (2001). https://doi.org/10.1016/S0022-3115(00)00554-7
31. A. Lyssoivan et al., Development of ICRF wall conditioning technique on divertor-type tokamaks ASDEX Upgrade and JET, J. Nucl. Mater. **337–339**, 456 (2005). https://doi.org/10.1016/j.jnucmat.2004.07.060
32. V.E. Moiseenko et al., Radio-frequency plasma start-up at Uragan-3M stellarator, Probl. Atom. Sci. Technol. **1**, 54 (2017).
33. V.E. Moiseenko et al., Threehalf-turn antennas start-up. Probl. Atom. Sci. Technol. **1**, 263 (2019).
34. M. Tripsky et al., A PIC-MCC code RFdinity1d for simulation of discharge initiation by ICRF antenna, Nucl. Fusion **57**, 126043 (2017). https://doi.org/10.1088/1741-4326/aa8446
35. V.E. Moiseenko , et al., Self-consistent modeling of radio-frequency plasma generation in stellarators, Plasma Phys. Rep. **39**, 873 (2013). https://doi.org/10.1134/S1063780X1311007X
36. Yu. S. Kulyk et al., Radio-frequency wall conditioning for steady-state stellarators. Probl. Atom. Sci. Technol. **6**, 56 (2016).
37. A. Lyssoivan et al., Simulation of ITER full-field ICWC scenario in JET: RF physics aspects. Plasma Phys. Control. Fusion **54**, 074014 (2012). https://doi.org/10.1088/0741-3335/54/7/074014
38. A. Lyssoivan et al., RF physics of ICWC discharge at high cyclotron harmonics. AIP Conf. Proc. **580**, 287 (2014). https://doi.org/10.1063/1.4864544
39. T. Wauters et al., 0D model of magnetized hydrogen–helium wall conditioning plasmas, Plasma Phys. Control. Fusion **53**, 125003 (2011). https://doi.org/10.1088/0741-3335/53/12/125003
40. A. Lyssoivan et al., Development of ICRF wall conditioning technique on divertor-type tokamaks ASDEX Upgrade and JET, J. Nucl. Mater. **337–339**, 456 (2005). https://doi.org/10.1016/j.jnucmat.2004.07.060
41. A. Lyssoivan et al., New scenarios of ICRF wall conditioning in TEXTOR and ASDEX Upgrade, J. Nucl. Mater. **363–365**, 1358 (2007). https://doi.org/10.1016/j.jnucmat.2007.01.186
42. M. K. Paul et al., Study of TEXTOR ICRF antenna coupling in the ICWC mode of operation, AIP Conf. Proc. **1187**, 177 (2009). https://doi.org/10.1063/1.3273722
43. A. Lyssoivan et al., Influence of toroidal and vertical magnetic fields on ion cyclotron wall conditioning in tokamaks, J. Nucl. Mater. **390–391**, 907 (2009). https://doi.org/10.1016/j.jnucmat.2009.01.233
44. Y. Kovtun et al., Comparison of ion cyclotron wall conditioning discharges in hydrogen and helium in JET, Nucl. Mater. Energy **37**, 101521 (2023). https://doi.org/10.1016/j.nme.2023.101521
45. D. R. Roberts, N. Hershkowitz, Enhanced slow-wave beach heating of mirror plasmas with two-ion species, Phys. Fluids B **4**, 1475 (1992). https://doi.org/10.1063/1.860058
46. Y. Yasaka et al., Observation of ion-cyclotron heating due to mode conversion of fast waves in a simple mirror, Phys. Fluids B **4**, 1486 (1992). https://doi.org/10.1063/1.860059
47. P. Y. Burchenko, E. D. Volkov, and E. D. Kramskoi, High-frequency plasma heating in a stellarator, JETP Lett. **15**, 174 (1972).
48. M. J. Hole et al., Global Alfven eigenmodes in the H-1 heliac, Plasma Phys. Controlled Fusion **59**, 125007 (2017), https://doi.org/10.1088/1361-6587/aa8bdf
49. V. E. Moiseenko et al., First experiments on ICRF discharge generation by a W7-X-like antenna in the Uragan-2M stellarator, J. Plasma Phys. **86**, 905860517 (2020). https://doi.org/10.1017/S0022377820001099
50. Y. V. Kovtun et al., ICRF plasma production in gas mixtures in the Uragan-2M stellarator, Fusion Eng. Des. **194**, 113887 (2023). https://doi.org/10.1016/j.fusengdes.2023.113887
51. A.V. Lozin et al., Uragan-2m gas mixing system, Probl. At. Sci. Technol. Ser.: Plasma Electronics and New Methods of Acceleration. **4**, 195 (2021). https://doi.org/10.46813/2021-134-195
52. V. E. Moiseenko et al., Plasma production in ICRF in the Uragan-2M stellarator in hydrogen–helium gas mixture, J. Fusion Energy **41**, 15 (2022). https://doi.org/10.1007/s10894-022-00326-8

53. Y. V. Kovtun et al., ICRF plasma production with the W7-X like antenna in the Uragan-2M stellarator, Plasma Fusion Res. **17**, 2402034 (2022). https://doi.org/10.1585/pfr.17.2402034
54. Y. V. Kovtun et al., ICRF plasma production with hydrogen minority heating in Uragan-2M and large helical device, Plasma Fusion Res. **18**, 2402042 (2023). https://doi.org/10.1585/pfr.18.2402042
55. Y. V. Kovtun et al., ICRF production of plasma with hydrogen minority in Uragan-2M stellarator by two-strap antenna, Phys. Plasmas **31**, 042501 (2024). https://doi.org/10.1063/5.0200911
56. Yu. V. Kovtun et al., Plasma behavior to hydrogen supersonic molecular beam injection in the Uragan-2M stellarator, Proceedings of the 49th EPS Conference on Plasma Physics, July 3 - 7 2023, Bordeaux, France, (2023), P1.057
57. Yu.V. Kovtun et al., Radio frequency plasma production at frequencies higher than ion cyclotron frequency at Uragan-2M stellarator, Proceedings of the 50th EPS Conference on Plasma Physics 2024 Salamanca, Jul 7 – 12, (2024), P2.077
58. R. Klima, A. V. Longinov, and K. N. Stepanov, High-frequency heating of plasma with two ion species, Nucl. Fusion **15**, 1157 (1975). https://doi.org/10.1088/0029-5515/15/6/021
59. Yu.V. Kovtun et al., ICRF plasma production in argon-hydrogen mixture in the Uragan-2M stellarator, Proceedings of the 24th International Stellarator Heliotron Workshop 9-13 September 2024, Hiroshima, Japan, ID 70
60. M. Osakabe et al., Current Status of Large Helical Device and Its Prospect for Deuterium Experiment. Fusion Science and Technology **72**, 199 (2017). http://dx.doi.org/10.1080/15361055.2017.1335145
61. S. Kamio et al., Study of ion cyclotron range of frequencies heating characteristics in deuterium plasma in the Large Helical Device, Nucl. Fusion **62**, 016004 (2022). http://dx.doi.org/10.1088/1741-4326/ac359d
62. H. Kasahara et al., The impact of ICRF heating using newly installed phasing antenna in LHD, Proceedings of the 38th EPS Conference on Plasma Physics (EPS, Strasbourg, 2011), Vol. 35G, P2.099
63. K. Saito et al., Field-aligned-impedance-transforming ICRF antenna in the LHD, Fusion Eng. Des. **96–97**, 583 (2015). https://doi.org/10.1016/j.fusengdes.2015.01.051
64. S. Kamio et al., First experiments on plasma production using field-aligned ICRF fast wave antennas in the large helical device, Nucl. Fusion **61**, 114004 (2021). https://doi.org/10.1088/1741-4326/ac277b
65. Y. V. Kovtun et al., ICRF plasma production at hydrogen minority regime in LHD, Nucl. Fusion **63**, 106002 (2023). https://doi.org/10.1088/1741-4326/acedc4
66. V. E. Moiseenko et al., ICRF plasma production and heating in LHD, Proceedings of the 29th IAEA Fusion Energy Conference (IAEA, 2023). 847.
67. V. E. Moiseenko et al., Ion cyclotron range of frequencies plasma production and heating in the large helical device, Phys. Plasmas **32**, 030701 (2025). https://doi.org/10.1063/5.0248769